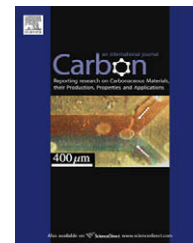


available at www.sciencedirect.comjournal homepage: www.elsevier.com/locate/carbon

Metal–organic framework (MOF) as a template for syntheses of nanoporous carbons as electrode materials for supercapacitor

Bo Liu ^{a,b}, Hiroshi Shioyama ^a, Hailong Jiang ^a, Xinbo Zhang ^a, Qiang Xu ^{a,b,*}

^a National Institute of Advanced Industrial Science and Technology (AIST), Ikeda, Osaka 563 8577, Japan

^b Graduate School of Engineering, Kobe University, Nada Ku, Kobe, Hyogo 657 8501, Japan

ARTICLE INFO

Article history:

Received 17 July 2009

Accepted 18 September 2009

Available online 24 September 2009

ABSTRACT

Five nanoporous carbons (NPCs) were prepared by polymerizing and then carbonizing carbon precursor of furfuryl alcohol accommodated in a porous metal–organic framework (MOF-5, $[\text{Zn}_4\text{O}(\text{bdc})_3]$, $\text{bdc} = 1,4\text{-benzenedicarboxylate}$) template. The Brunauer–Emmett–Teller (BET) surface areas for five NPC samples obtained by carbonizing at the temperatures from 530 to 1000 °C fall into the range from 1140 to 3040 $\text{m}^2 \text{g}^{-1}$ and the dependence of BET surface areas on carbonization temperatures shows a “V” shape. All the five NPC samples have a pore size distribution centered at about 3.9 nm. As electrode materials for supercapacitor, the NPC samples obtained at the temperatures higher than 600 °C display the ideal capacitor behaviors and give rise to almost constant specific capacitance (above 100 F g^{-1} at 5 mV s^{-1}) at various sweep rates, which is associated with their mesoporous characteristics. However, the NPC sample with the highest BET surface area (3040 $\text{m}^2 \text{g}^{-1}$) obtained by carbonizing at 530 °C gives a unusually low capacitance (12 F g^{-1} at 5 mV s^{-1}), which may be attributed to the poor conductivity of the carbon material due to the low carbonization temperature.

© 2009 Elsevier Ltd. All rights reserved.

1. Introduction

Nanoporous carbon (NPC) materials with high surface area have been widely applied in many fields such as adsorbents [1], catalyst supports [2], and electrode materials [3]. Extensive methods have been employed to prepare carbon materials, including laser ablation [4], electrical arc [5], chemical vapor decomposition (CVD) [6], and templating [7,8] as well as chemical or physical activation methods [9], among which, the template method is an effective way to prepare nanoporous carbon materials. A templating process generally includes three main steps: (i) preparation of precursor/template composite; (ii) transformation of the precursor to the target product; and (iii) removal of the template. Two different template modes, endotemplate and exotemplate [10],

can be distinguished according to the function of the template. In the endotemplate case, the template such as silica nanoparticles is embedded into the precursor and a pore system was generated after removal of the template. In the exotemplate case, a precursor is introduced into the pores of the template. In this way, either a small particle or a porous solid is generated, depending on the connectivity of the exotemplate. With template methods, ordered mesoporous carbon molecular sieves have been prepared via carbonizing sucrose precursor filled in the ordered mesoporous silica template using sulfuric acid as a catalyst, and the carbon replica of the MCM-48 mesophase has also been obtained with phenol–formaldehyde as carbon precursor [11,12]. An ordered microporous carbon that preserves the structural regularity of Y zeolite has also been reported using Y zeolite as a

* Corresponding author. Address: National Institute of Advanced Industrial Science and Technology (AIST), 1-8-31 Midorigaoka, Ikeda, Osaka 563 8577, Japan. Fax: +81 72 751 7942.

E-mail address: q.xu@aist.go.jp (Q. Xu).

0008-6223/\$ - see front matter © 2009 Elsevier Ltd. All rights reserved.

doi:10.1016/j.carbon.2009.09.061

template with a two-step method [13]. High porosity and thermal stability are required for materials to behave as exotemplates, for example zeolites and ordered mesoporous silica.

On the other hand, metal–organic frameworks (MOFs) as a kind of emerging nanoporous material have attracted many attentions due to their intriguing architectures and topologies, tunable pore sizes, and wide potential applications such as gas storage and separation, drug delivery, and so on [14–21]. The various pore sizes and high thermal stability of MOFs make them feasible as templates for preparing nanoporous carbon materials. In our recent proclaiming work, we have introduced furfuryl alcohol (FA) vapor into the pores of MOF-5 ($[\text{Zn}_4\text{O}(\text{bdc})_3]$, bdc = 1,4-benzenedicarboxylate) followed by polymerization and carbonization to prepare a nanoporous carbon material, which shows excellent electrochemical performance as an electrode material for supercapacitor [21]. In the present work, we introduced furfuryl alcohol into the pores of MOF-5 by employing incipient wetness technique to prepare nanoporous carbon materials. With different methods to introduce FA precursor, the structures of the resultant carbon materials are quite distinct. The structural evolution of the NPC samples with increasing temperature and their electrochemical performances as electrode materials for supercapacitor are discussed in detail.

2. Experimental

2.1. Syntheses of nanoporous carbons (NPCs)

Five nanoporous carbon materials were synthesized using MOF-5 as a template. The synthesis strategy of using MOF-5 as a template and furfuryl alcohol (FA) as a carbon precursor has been described previously, in which FA was introduced into the pores of MOF-5 by means of FA vapor [21]. In this work, the incipient wetness technique was employed for introducing carbon precursor of FA. MOF-5 was prepared according to the reported method [22]. The as-prepared MOF-5 was degassed at 200 °C for 3 h to remove the solvent molecules accommodated in the pores of MOF-5. The degassed MOF-5 was soaked in the FA and the mixture was pumped for 40 min and then stood overnight in order to fully infiltrate FA into the pores of MOF-5, followed by filtrating and washing with DMF to remove the FA adhesive to the outer surface of MOF-5. Subsequently, the FA/MOF-5 composite was transferred into a quartz boat. After excluding air by flowing Ar gas for 6 h, the FA accommodated in the pores of MOF-5 was polymerized by heating at 80 °C for 24 h and then 150 °C for 6 h in an Ar flow. Subsequent carbonization at 530, 650, 800, 900, and 1000 °C for 8 h for each sample was carried out to give rise to the formation of the five nanoporous carbon (NPC) samples. Correspondingly, the as-prepared NPC samples are denoted as as-NPC₅₃₀, as-NPC₆₅₀, as-NPC₈₀₀, NPC₉₀₀, and NPC₁₀₀₀. The as-prepared NPC samples of as-NPC₅₃₀, as-NPC₆₅₀, and as-NPC₈₀₀ were treated with HCl aqueous solution (0.1 M) to remove ZnO resulting from the decomposition of MOF-5 template. The treated samples were denoted to NPC₅₃₀, NPC₆₅₀, and NPC₈₀₀, respectively.

2.2. Characterization

The powder X-ray diffraction (PXRD) measurements were performed by using Cu K α radiation (40 kV, 40 mA, $\lambda = 1.54050 \text{ \AA}$) with a speed of 0.02 s⁻¹ on an X-ray diffractometer (Rigaku, Rint 2000). The nitrogen adsorption/desorption experiments were investigated at liquid nitrogen temperature (–196 °C) by using an automatic volumetric adsorption equipment (Micromeritics, ASAP 2010). BET surface areas were determined over a relative pressure range of 0.05–0.20, during which the BET plot is linear; meso and macropore volumes were calculated using adsorption isotherms by BJH method and micropore volume was determined by subtracting meso and macropore volumes calculated by BJH method from total pore volume. Before measurements, all the samples were degassed at 150 °C for 3 h.

2.3. Electrode preparation and electrochemical performance test

All electrochemical measurements were carried out in a two-electrode cell (capacitor) with 1.0 M sulfuric acid aqueous solution as electrolyte (each electrode with an apparent electrode area of 1 cm² containing 2.0 mg of active material NPC without adding any binder and conductive agents), in which a glassy paper separator was sandwiched between two electrodes and Pt plates were used as current collectors. The electrochemical experiments have also been carried out for NPC₆₅₀ as a representative with a much larger amount (8.0 mg) on each electrode, keeping all other experimental conditions the same. The results indicate that the electrochemical performance does not depend on the amount of the carbon materials used. Two symmetry electrodes were adopted as cathode and anode for the cell configuration.

All the electrochemical experiments were performed at ambient temperature. Before the measurements, the capacitor cell was soaked in electrolyte and evacuated for 30 min so that the active material was infiltrated fully by the electrolyte. Cyclic voltammograms at different sweep rates between –0.5 and 0.5 V for the capacitors were carried out on an automatic polarization system (Hokuto Denko, HZ 5000). Galvanostatic charge/discharge tests at various current densities between –0.5 and 0.5 V were performed on an electrochemical interface (Solartron, S1 1287).

3. Results and discussion

3.1. Structural evolution of nanoporous carbon materials

Powder X-ray diffraction patterns of as-NPC₅₃₀, as-NPC₆₅₀, and as-NPC₈₀₀ were shown in Fig. 1a, where all the main peaks are attributed to the ZnO deriving from the decomposition of the MOF-5 template. Carbon signals can be observed after removing of ZnO by treating the three as-prepared NPC samples with HCl aqueous solution (Fig. 1b). However, for the samples obtained by carbonizing at the temperature higher than 900 °C, signals of ZnO species cannot be found in the PXRD patterns (Fig. 1b). This phenomenon has been explained in our previous work [21]. During the carbonization process,

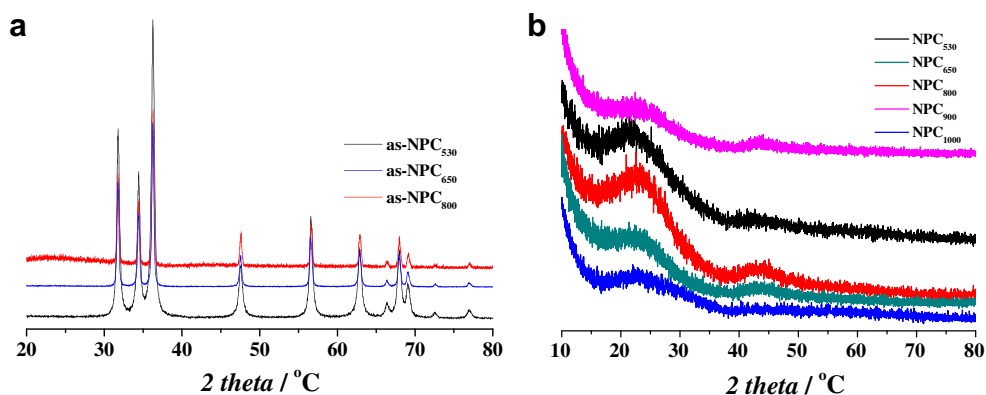


Fig. 1 – Powder XRD patterns for (a) as-NPC₅₃₀, as-NPC₆₅₀, and as-NPC₈₀₀, in which all the main peaks are attributed to the ZnO resulting from the decompositions of the MOF-5 template and (b) NPC₅₃₀, NPC₆₅₀, NPC₈₀₀, NPC₉₀₀, and NPC₁₀₀₀ samples.

MOF-5 was decomposed to ZnO at the temperature higher than 500 °C; with temperature further increasing to higher than 800 °C, ZnO was reduced to metallic Zn species [23], and subsequently, Zn metal (boiling point 908 °C) vaporized away along with the Ar flow, leaving carbon species alone in the resulting NPC samples (NPC₉₀₀ and NPC₁₀₀₀), which is consistent with the PXRD result. The PXRD patterns for the five NPC samples display two broad peaks at $2\theta = 23^\circ$ and 44° , corresponding to the diffractions for carbon.

3.2. Nitrogen adsorption analysis

Nitrogen adsorption–desorption isotherms as shown in Fig. 2a were measured to evaluate the surface area and the pore size distribution of the five NPC samples. The detailed data are summarized in Table 1. The general shape of the N₂ sorption isotherms for all the NPC samples suggests the existence of different pore sizes spanning from micro to macropores. Hysteresis between adsorption and desorption branches can be observed at medium relative pressure for all the samples, which demonstrates the existence of mesopores. The almost vertical tails at the relative pressure near to 1.0 point to the presence of macroporosity. The ratio of micropore is low for all the samples. Pore size distributions of the five NPC sam-

ples calculated from the nitrogen adsorption branches are shown in Fig. 2b. The majority of pores are located in the region of mesopore. All the samples display very close pore size distribution with a peak centering at ca. 4.0 nm. The nitrogen sorption characteristic of those NPC samples is much different with nanoporous carbon material reported in our previous work, for which the micropores ratio is up to 25%, with a negligible macropores [21].

The relationship between specific surface area (BET and Langmuir) and the carbonization temperature is shown in Fig. 3. The “V” shape curve indicates that carbonization temperature has a complicated effect for the carbonization process. It has been reviewed that polymerized FA-derived carbon changes from disordered to ordered structure with increasing carbonization temperature and/or longer carbonization period [24]. However, in the present case, the formation of the carbon structure is more intricate due to the decomposition of MOF-5 template during the carbonization process. According to the TG analysis, the MOF-5 decomposes into ZnO at the temperature higher than 500 °C in an Ar flow [21]. As observed in the PXRD patterns, when the carbonization temperature is lower than 900 °C, ZnO species remains. At 530 °C, the decomposition of MOF-5 is completed; the removal of ZnO by washing with HCl aqueous solution leaves

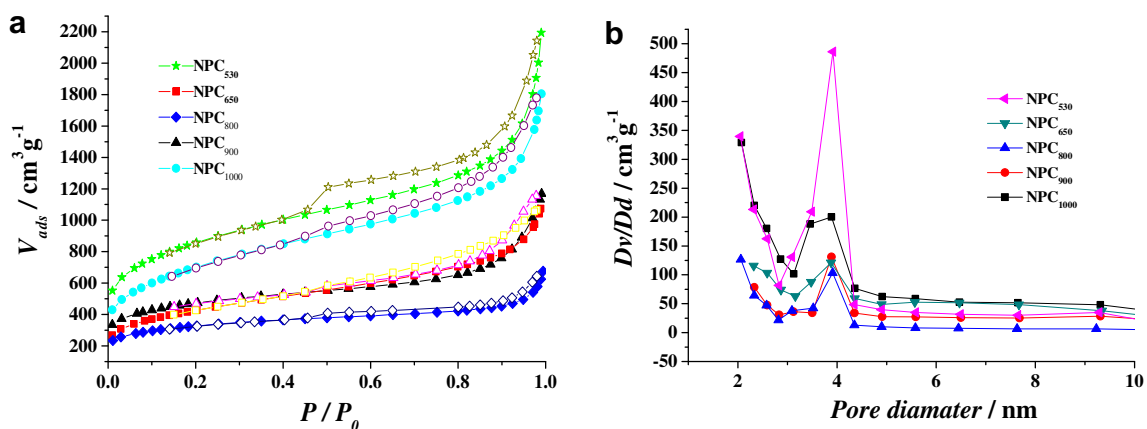


Fig. 2 – (a) Nitrogen adsorption–desorption isotherms and (b) pore size distributions calculated from N₂ adsorption isotherms for NPC samples. The open and closed symbols refer to adsorption and desorption branches, respectively.

Table 1 – BET surface areas (*S*), pore volumes (*V*) and pore sizes (*D*) for the five NPC samples.

Samples	<i>S</i> (m ² g ⁻¹)	<i>V</i> (cm ³ g ⁻¹)				<i>D</i> ^c (nm)
		<i>V</i> _{total} ^a	<i>V</i> _{micro} ^b	<i>V</i> _{meso} ^b	<i>V</i> _{macro} ^b	
NPC ₅₃₀	3040	2.79	0	2.14	0.65	3.7
NPC ₆₅₀	1521	1.48	0.06	1.23	0.19	3.9
NPC ₈₀₀	1141	0.84	0.12	0.50	0.22	2.9
NPC ₉₀₀	1647	1.57	0.2	1.11	0.26	3.9
NPC ₁₀₀₀	2524	2.44	0.01	2.05	0.38	3.9

^a The pore volume is calculated at a relative pressure of 0.97.

^b Meso and macropores volumes are calculated using adsorption isotherms by BJH method and micropore volume is determined by subtracting meso and macropore volumes calculated by BJH method from total pore volume.

^c The pore diameter is referred to the pore size corresponding to the peak position in Fig. 2b.

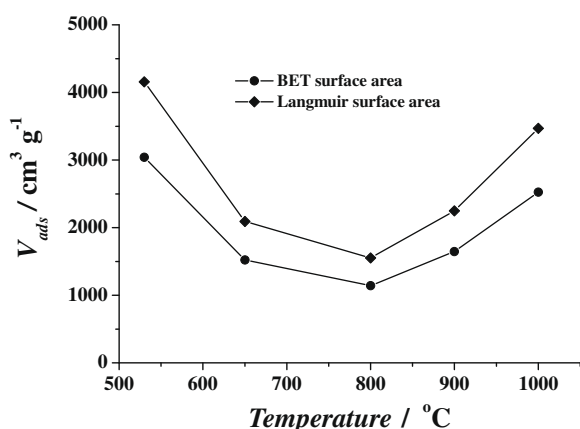


Fig. 3 – The relationship between surface areas (BET and Langmuir) and the carbonization temperatures for NPC samples.

the nanoporous pores. For the NPC₅₃₀, the highest specific surface area (3040 m² g⁻¹) is obtained. With the temperature increasing to 650 and 800 °C, the specific surface areas were decreased to 1521 and 1141 m² g⁻¹, respectively. However, subsequent reduction of ZnO and Zn vaporizing at the temperature higher than 800 °C further results in the surface area increasing to 1647 and 2524 m² g⁻¹ at 900 and 1000 °C, respectively. In this process, the role of Zn vapor may be similar with that of water vapor in a chemical activation process.

3.3. Electrochemical properties of nanoporous carbons as electrode materials for supercapacitor

In an electrochemical capacitor, the charge is accumulated in the double layers mainly by electrostatic force. The energy is stored based on the separation of charged species across the electrode–electrolyte interface. The value of capacitance is strictly connected with the nature and surface of the electrodes as well as the interaction between electrode and electrolyte. Generally, the specific capacitance is proportional to the specific surface area of electrode ($C = \epsilon S/d$, ϵ is the permittivity of the electrolyte, S is the surface area of the electrode–electrolyte interface, and d is the distance between the polarized electrode surface and the maximum charge density of the solvated ions) [25,26]. However, only the surface which

can be electrochemically accessed by the solvated ions makes contribution to the capacitance. The pore dimensions should be adapted to the sizes of the solvated ions. In addition, the surface wettability and the conductivity of the electrode also have great effect for an optimized performance of a capacitor.

Two-electrode NPC-based capacitors cycling potentiodynamically between -0.5 and 0.5 V at various sweep rates was adopted to evaluate the specific capacitances for all the five NPC samples. It is noteworthy that the electrode is made up from only the NPC samples without adding any binder and conductive reagents. The specific capacitance is calculated according to $C = 2 \times I / (S \times m)$, where I is the current value at 0 V, S is the sweep rate, and m is the mass of carbon on an electrode. The factor of two in the equation comes from the fact that the total capacitance measured from the test cells is the sum of two equivalent single electrode capacitors in series. The specific capacitances at different sweep rates are shown in Fig. 4 and summarized in Table 2 for the five NPC samples. For the samples carbonized above 600 °C, the specific capacitances do not change obviously when the sweep rates increase from 5 to 50 mV s⁻¹ (Fig. 4). This characteristic is associated with the mesoporous feature of the NPC samples. The mesopores can be accessed freely and quickly by electrolyte ions. Even at a high sweep rate of 50 mV s⁻¹, no diffusion limitation can be observed. For NPC₁₀₀₀ sample, the cyclic voltammetrical curves at various sweep rates behave as approximately perfect rectangular shape, which corresponds to the ideal capacitor behavior. Besides NPC₅₃₀, other NPC samples also display regular rectangular shapes at various sweep rates. At the sweep rate as high as 50 mV s⁻¹, the specific capacitance reaches up to 152 F g⁻¹ for NPC₆₅₀ and about 100 F g⁻¹ for other samples, which indicates an excellent energy and power densities for NPC samples.

Unexpectedly, the NPC₅₃₀ with the highest specific surface area as high as 3040 m² g⁻¹ and a major mesopore gives rise to an incredibly low capacitance value. This phenomenon may be induced from the poor electrical conductivity of the NPC sample prepared by carbonizing at low temperature. As mentioned above, no conductivity agents were used for present capacitance measurements. It has been reported that electrical conductivity of polymerized FA-derived carbon materials increase with the elevated carbonization temperature, and a trend of semiconductor-to-metal transition appears at or above a pyrolytic temperature of 850 °C [24]. This characteristic is verified by the sharp voltage drop at the

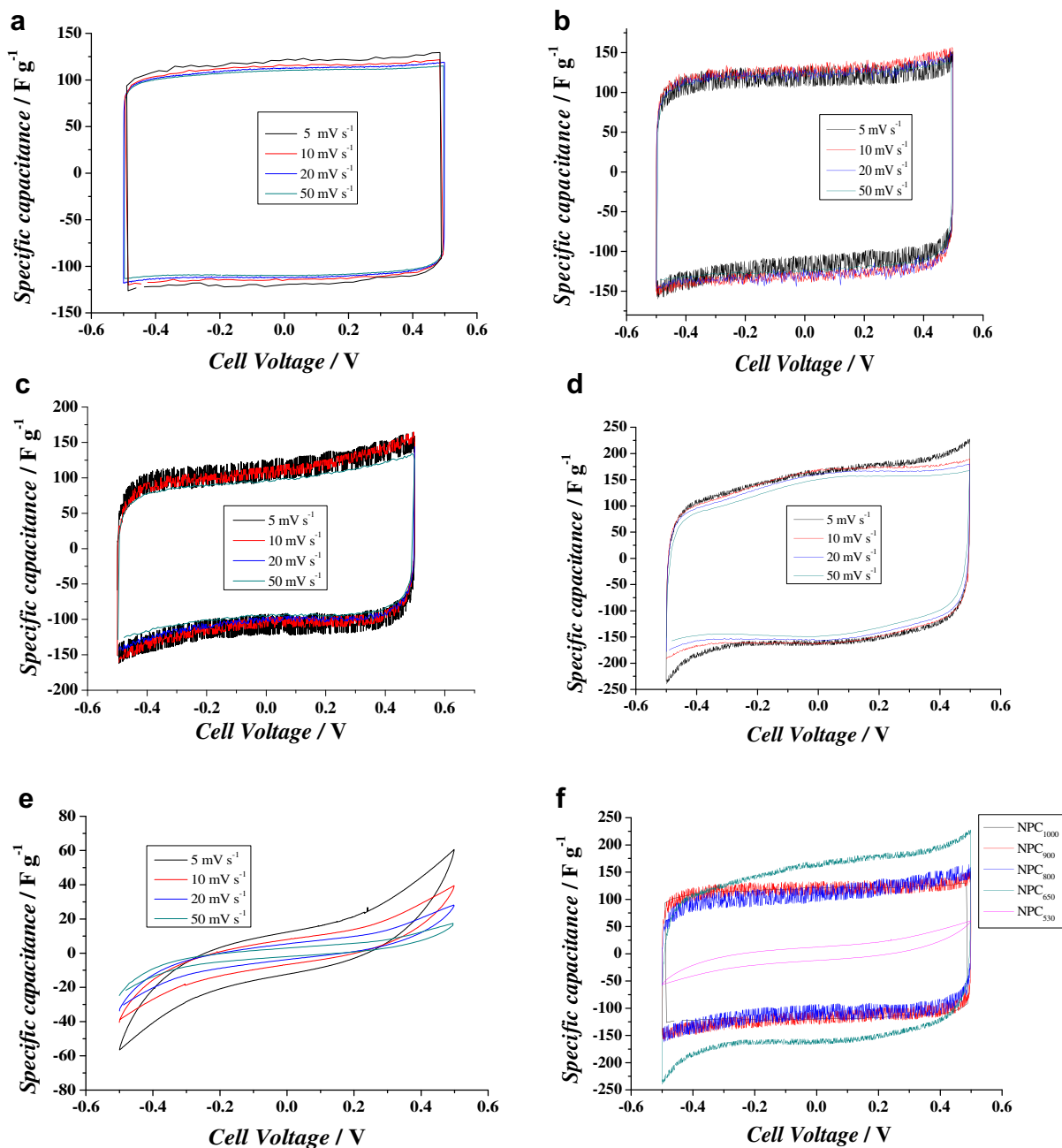


Fig. 4 – Cyclic voltammograms at different sweep rates (5–50 mV s^{-1}) for NPC samples: (a) NPC₁₀₀₀, (b) NPC₉₀₀, (c) NPC₈₀₀, (d) NPC₆₅₀, (e) NPC₅₃₀, and (f) comparison of the cyclic voltammograms at 5 mV s^{-1} for five NPC samples. The Y axis is normalized to specific capacitance.

Table 2 – Specific capacitance at different sweep rates and current densities for the five NPC samples.

Samples	Specific capacitance (F g^{-1})							
	Sweep rate (mV s^{-1})				Current density (mA g^{-1})			
	5	10	20	50	50	100	250	500
NPC ₅₃₀	12	8	6	3	158	134	48	11
NPC ₆₅₀	167	165	162	152	222	203	195	188
NPC ₈₀₀	107	102	98	97	151	127	122	112
NPC ₉₀₀	122	119	126	123	148	138	123	116
NPC ₁₀₀₀	120	115	112	110	149	139	129	118

beginning of the discharge in the constant current charge/discharge process. It is believed that the sharp voltage drop is due to the high equivalent series resistance (ESR). However, with the same materials and assembling process for the capacitors, other NPC samples do not show such an obvious voltage drop. Hence, the conclusion may be drawn that the sharp voltage drop comes from the poor electrical conductivity of NPC₅₃₀ due to the low carbonization temperature.

Galvanostatic charge/discharge between -0.5 and 0.5 V has also been employed to estimate the electrochemical performance of NPC samples as electrode materials for superca-

pacitor (Fig. 5). Specific capacitance of each electrode was calculated according to $C = 2 \times I \times \Delta t / (\Delta V \times m)$, where I is the discharge current, Δt , the discharge time from 0 to -0.5 V, ΔV , the voltage difference within the discharge time Δt , and m , the mass of carbon on an electrode. The factor of two in this equation also comes from the fact that the total capacitance measured from the test cells is the sum of two equivalent single electrode capacitors in series. The specific capacitances for five NPC samples at various current densities are summarized in Table 2. No obvious voltage drop can be observed at the beginning of the discharge process for NPC

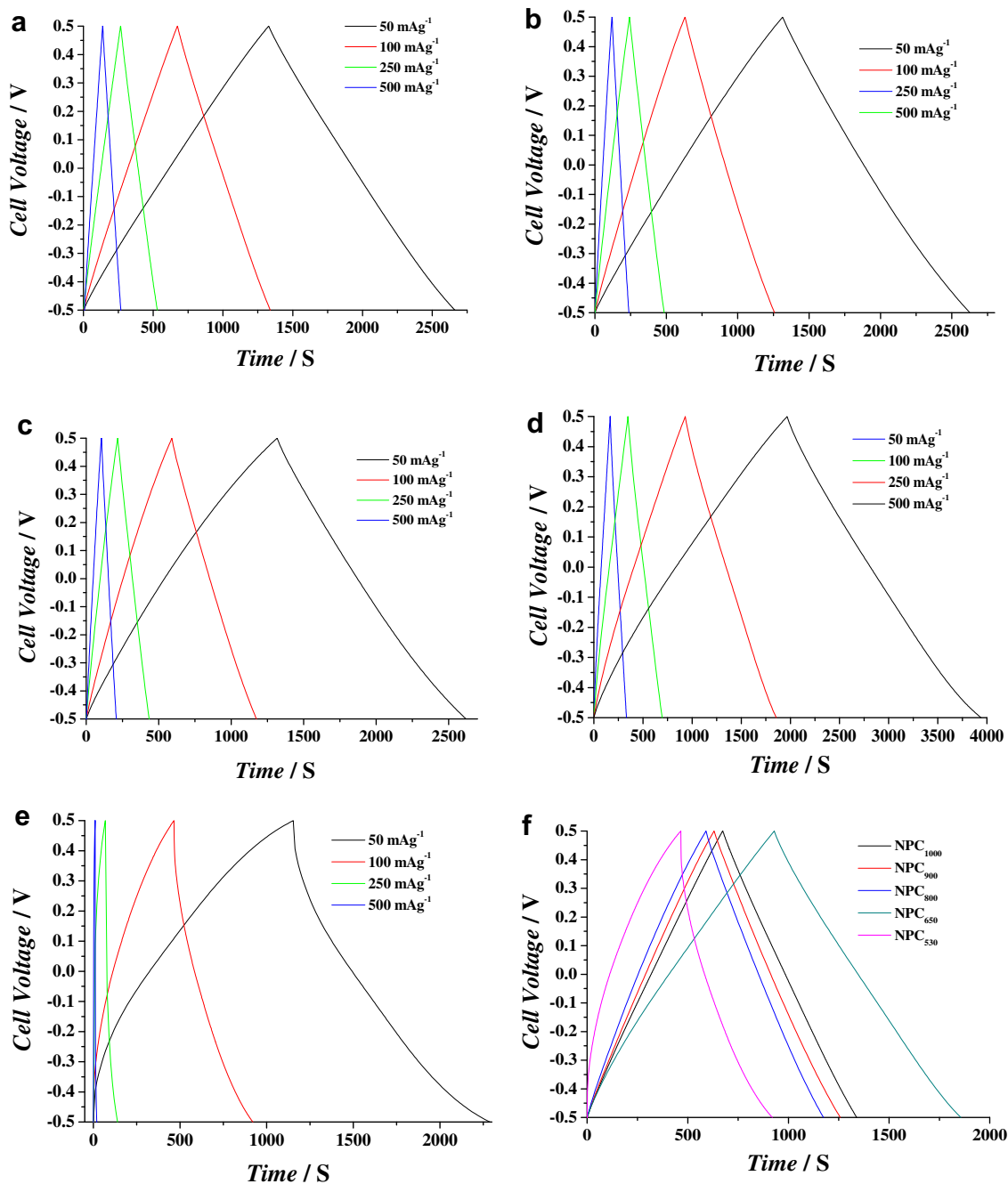


Fig. 5 – Galvanostatic charge/discharge curves at different current densities for NPC samples: (a) NPC₁₀₀₀, (b) NPC₉₀₀, (c) NPC₈₀₀, (d) NPC₆₅₀, (e) NPC₅₃₀, and (f) comparisons of the galvanostatic charge/discharge curves at the current density of 100 mA g^{-1} for five NPC samples.

samples obtained by carbonizing above 600 °C and all the samples display regularly triangular shapes at various current densities. The feature indicates the good columbic efficiency and ideal capacitor behavior, consistent with the result of voltammetrical experiments. As mentioned above, the NPC₅₃₀ gives rise to a sharp voltage drop compared with other NPCs, which leads to its poor electrochemical performance as electrode material for supercapacitor. NPC₆₅₀ gives a highest specific capacitance of 222 F g⁻¹ at a current density of 50 mA g⁻¹. Fig. 5f shows the constant current charge/discharge curves for five NPC samples at a current density of 100 mA g⁻¹. Excellent performance of carbon-based capacitor depends on the high surface area and controlled pore sizes as well as good conductivity. For the nanoporous carbon reported in our previous work, the specific capacitance decays ca. 22% (from 204 to 159 F g⁻¹) with the increasing sweep rates from 5 to 50 mV s⁻¹, which is associated with the diffusion limitation within the micropores. In this work, nanoporous carbon materials mainly with mesopores were synthesized. The capacitances keep almost constant when the sweep rates increase from 5 to 50 mV s⁻¹. It is clear that pore structures of prepared carbon materials depend on the methods for introducing carbon precursors. Using vapor method, the obtained carbon materials contains large ratio of micropores (up to ~25%), while the micropores is quite low in the sample prepared by incipient wetness method in present work. Subsequently, the difference of pore structures results in the different electrochemical behaviors as electrode materials for supercapacitor. It is well known that micropore system is beneficial to the improvement of energy density, while the mesopore system favors the enhancement of power density. In this sense, the electrochemical performance of the carbon materials prepared by MOF template route can be controlled by adopting different methods for introducing carbon precursors.

4. Conclusions

In summary, we have employed a metal–organic framework (MOF-5) as a template to prepare nanoporous carbons, which exhibits high specific surface areas mainly with mesopores and excellent electrochemical properties as electrode materials for supercapacitor. The specific surface area, pore size distribution, and electrical conductivity of the resultant carbon materials are influenced by the carbonization temperature. These factors result in the varied electrochemical response of NPC samples as electrode materials for supercapacitor. The carbons obtained at higher temperature (for example, 1000 °C) give rise to ideal capacitor behaviors owing to their high mesoporosities and good electrical conductivity. However, the carbon material obtained at lower temperature (530 °C) shows poor electrochemical performance due to its poor electrical conductivity. The highest specific capacitances are obtained for NPC₆₅₀ as high as 167 and 222 F g⁻¹ at a sweep rate of 5 mV s⁻¹ and a current density of 50 mA g⁻¹, respectively. Furthermore, the specific capacitance shows little decrease with the increasing sweep rates and current densities. The present finding provides us a new example of application of the rapidly growing MOF family. The structural

diversity of MOFs may show high potential as templates for synthesizing functional carbon materials.

Acknowledgements

We thank editor and the reviewers for their valuable comments and suggestions and AIST and Kobe University for the financial support. B. Liu thanks MEXT for Japanese Government Scholarship.

REFERENCES

- [1] Suda H, Haraya K. Alkene/alkane permselectivities of a carbon molecular sieve membrane. *Chem Commun* 1997;32(1):93–4.
- [2] Rodeiquez-Reinoso F. The role of carbon materials in heterogeneous catalysis. *Carbon* 1998;36(3):159–75.
- [3] Maruyama J, Sumino K, Kawaguchi M, Abe I. Influence of activated carbon pore structure on oxygen reduction at catalyst layers supported on rotating disk electrodes. *Carbon* 2004;42(15):3115–21.
- [4] Thess A, Lee R, Nikolaev P, Dai H, Petit P, Robert J, et al. Crystalline ropes of metallic carbon nanotubes. *Science* 1996;273(5274):483–7.
- [5] Journet C, Maser WK, Bernier P, Loiseau A, Chapelle ML, Lefrant S, et al. Large-scale production of single-walled carbon nanotubes by the electric-arc technique. *Nature* 1997;388(6644):756–8.
- [6] Zheng B, Lu C, Gu G, Makarovski A, Finkelstein G, Liu J. Efficient CVD growth of single-walled carbon nanotubes on surfaces using carbon monoxide precursor. *Nano Lett* 2002;2(8):895–8.
- [7] Yang Q, Xu W, Tomita A, Kyotani T. The template synthesis of double coaxial carbon nanotubes with nitrogen-doped and boron-doped multiwalls. *J Am Chem Soc* 2005;127(25):8956–7.
- [8] Kim T-W, Park I-S, Ryoo R. Intramolecular aromatic amination through iron-mediated nitrene transfer. *Angew Chem Int Ed* 2003;42(36):4360–75.
- [9] Ahmadpour A, Do DD. The preparation of active carbons from coal by chemical and physical activation. *Carbon* 1996;34(4):471–9.
- [10] Schüth F. Endo- and exotemplating to create high-surface-area inorganic materials. *Angew Chem Int Ed* 2003;42(31):3604–22.
- [11] Ryoo R, Joo SH, Jun S. Synthesis of highly ordered carbon molecular sieves via template-mediated structural transformation. *J Phys Chem B* 1999;103(37):7743–6.
- [12] Lee J, Yoon S, Hyeon T, Oh SM, Kim KB. Synthesis of a new mesoporous carbon and its application to electrochemical double-layer capacitors. *Chem Commun* 1999;34(21):2177–8.
- [13] Ma Z, Kyotani T, Tomita A. Preparation of a high surface area microporous carbon having the structural regularity of Y zeolite. *Chem Commun* 2000;23:2365–6.
- [14] Li H, Eddaoudi M, O’Keeffe M, Yaghi OM. Design and synthesis of an exceptionally stable and highly porous metal–organic framework. *Nature* 1999;402(6759):276–9.
- [15] Chen B, Eddaoudi M, Hyde ST, O’Keeffe M, Yaghi OM. Interwoven metal–organic framework on a periodic minimal surface with extra-large pores. *Science* 2001;291(5506):1021–3.
- [16] Pan L, Parker B, Huang XY, Olson DH, Lee J-Y, Li J. Zn(tbip) (H₂tbip = 5-tert-Butyl Isophthalic Acid): a highly stable guest-free microporous metal organic framework with unique gas separation capability. *J Am Chem Soc* 2006;128(13):4180–1.

- [17] Zou RQ, Sakurai H, Xu Q. Charge transport in three-terminal molecular junctions incorporating sulfur-end-functionalized tercyclohexylidene spacers. *Angew Chem Int Ed* 2006;45(16):2540–2.
- [18] Zou RQ, Sakurai H, Han S, Zhong RQ, Xu Q. Probing the Lewis acid sites and CO catalytic oxidation activity of the porous metal–organic polymer [Cu(5-methylisophthalate)]. *J Am Chem Soc* 2007;129(27):8402–3.
- [19] Mulfort KL, Hupp JT. Chemical reduction of metal–organic framework materials as a method to enhance gas uptake and binding. *J Am Chem Soc* 2007;129(31):9604–5.
- [20] Schröder F, Esken D, Cokoja M, van denBerg MWE, Lebedev OI, Tendeloo GV, et al. Ruthenium nanoparticles inside porous $[Zn_4O(bdc)_3]$ by hydrogenolysis of adsorbed $[Ru(cod)(cot)]$: a solid-state reference system for surfactant-stabilized Ruthenium Colloids. *J Am Chem Soc* 2008;130(19):6119–30.
- [21] Liu B, Shioyama H, Akita T, Xu Q. Metal–organic framework as a template for porous carbon synthesis. *J Am Chem Soc* 2008;130(16):5390–1.
- [22] Gonzalez J, Devi RN, Tunstall DP, Cox PA, Wright PA. Deuterium NMR studies of framework and guest mobility in the metal–organic framework compound MOF-5, $Zn_4O(O_2CC_6H_4CO_2)_3$. *Micropor Mesopor Mater* 2005; 84(1–3):97–104.
- [23] Fletcher EA. Solar thermal and solar quasi-electrolytic processing and separations: zinc from zinc oxide as an example. *Ind Eng Chem Res* 1999;38(6): 2275–82.
- [24] Wang H, Yao J. Use of poly(furfuryl alcohol) in the fabrication of nanostructured carbons and nanocomposites. *Ind Eng Chem Res* 2006;45(19):6393–404.
- [25] Lozano-Castello D, Cazorla-Amoros D, Linares-Solano A, Shiraishi S, Kurihara H, Oya A. Influence of pore structure and surface chemistry on electric double layer capacitance in non-aqueous electrolyte. *Carbon* 2004;41(3):1765–75.
- [26] Shi H. Activated carbons and double layer capacitance. *Electrochim Acta* 1996;41(10):1633–9.